

Image Mosaicing and Super-resolution

Dario Comanducci, 12 aprile 2024

1 Introduction

Super-resolution restoration aims to solve the following problem: given a set of observed images, estimate an image at a higher-resolution than is present in any of the individual images.

The approach discussed in [1, 2] is outlined in Fig. 1. The input images are first mutually aligned onto a common reference frame. This alignment involves not only a geometric component, but also a photometric component, modelling illumination, gain or colour balance variations among the images. After alignment a composite image mosaic may be rendered and super-resolution restoration may be applied to any chosen region of interest.

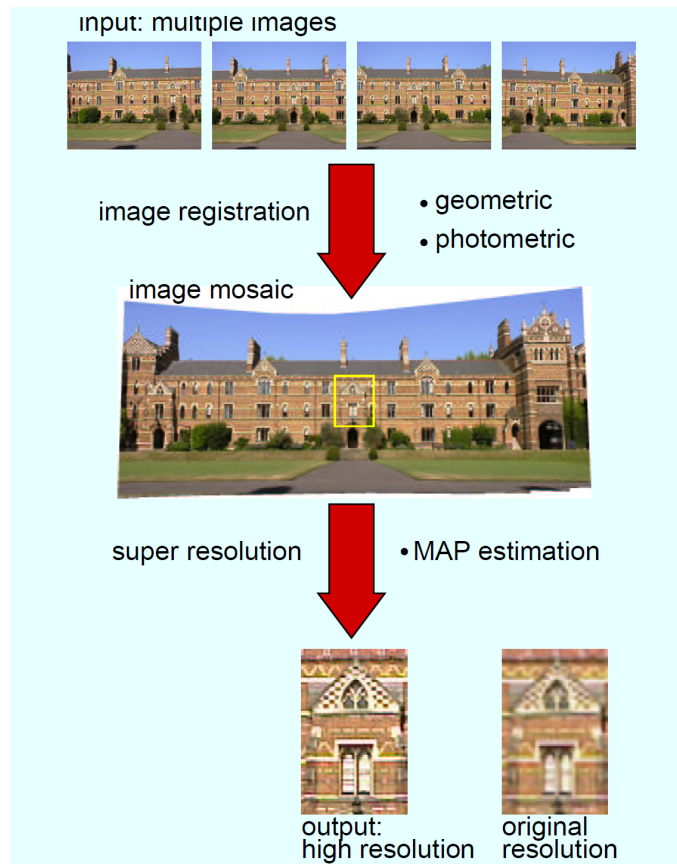


Fig. 1: Stages in the super-resolution process.

The two key components of the approach are:

- the accurate alignment or *registration* of the low-resolution images (§ 2);
- and the formulation of a super-resolution estimator exploiting a generative image model together with a prior model of the super-resolved image (§ 3).

2 Image registration

Essential to the success of any super-resolution algorithm is the need to find a highly accurate point-to-point correspondence or registration between images in the input sequence. This correspondence problem can be stated as follows: *given two different views of the same scene, for each image point in one view find the image point in the second view which corresponds to the same actual point in the scene.*

2.1 Image registration model

We will focus on the case of images which are related by a planar projective transformation, also called a *planar homography*, a geometric transformation which has 8 degrees of freedom. Under a planar homography a point $q = (x, y)$ is mapped in $q' = (x', y')$ as

$$x' = \frac{h_{11}x + h_{12}y + h_{13}}{h_{31}x + h_{32}y + h_{33}} \quad (1a)$$

$$y' = \frac{h_{21}x + h_{22}y + h_{23}}{h_{31}x + h_{32}y + h_{33}} \quad (1b)$$

In the following, Eq. (1) will be denoted as $\mathbf{q}' = \mathbf{H}\mathbf{q}$ by exploiting homogeneous coordinates (see appendix A for details).

There are two important situations in which a planar homography is appropriate (Fig. 2):

- images of a plane viewed under arbitrary camera motion;¹
- and images of an arbitrary 3D scene viewed by a camera rotating about its optic centre and/or zooming.

In both cases, the image points $q = (x, y)$, and $q' = (x', y')$, correspond to a single point Q in the world.

2.2 Homography estimation

Typically, in each image several hundred “interest points” are automatically detected with sub-pixel accuracy (Figs. 3a, 3b): putative correspondences between each pair of images are then identified by comparing local descriptors based on the image neighbourhoods around the features (Fig. 3c).

¹ This can occurs also when a freely moving camera views a very distant scene, such as is the case in high-aerial or satellite photography: because the distance of the scene from the camera is very much greater than the motion of the camera between views, the parallax effects caused by the three dimensional nature of the scene are negligibly small.

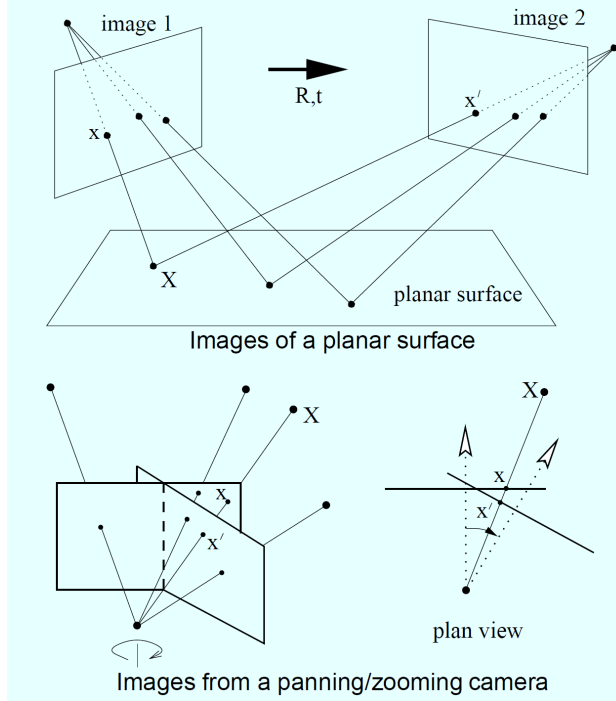


Fig. 2: Scenarios for which the image-to-image correspondence is captured by a planar homography.

In order to remove outliers, these correspondences are refined using a robust search procedure such as the RANSAC algorithm [3, pp. 117-121] which extracts only those features whose inter-image point motion is consistent with a homography (Fig. 3d).

2.2.1 Image pairwise registration by Maximum Likelihood

The inlying correspondences found by RANSAC are used in a non-linear *Maximum Likelihood* (ML) estimator which returns a highly accurate estimate of the homography.

Once outliers have been removed, the assumption of a Gaussian error model, even if not strictly justified, is quite tenable. Therefore, for the present, we assume that image measurement errors obey an isotropic Gaussian distribution with zero mean and standard deviation σ : given a true, noise-free point $\bar{q} = (\bar{x}, \bar{y})$, the probability density function (PDF) of each measured point $q = (x, y)$ is

$$p(q|\bar{q}) = \frac{1}{2\pi\sigma^2} \exp \left(-\frac{d(q, \bar{q})^2}{2\sigma^2} \right) = \frac{1}{2\pi\sigma^2} e^{-d(q, \bar{q})/\sigma^2}$$

Furthermore, we can make the very reasonable assumptions that

- the feature localization error is uncorrelated across different images;

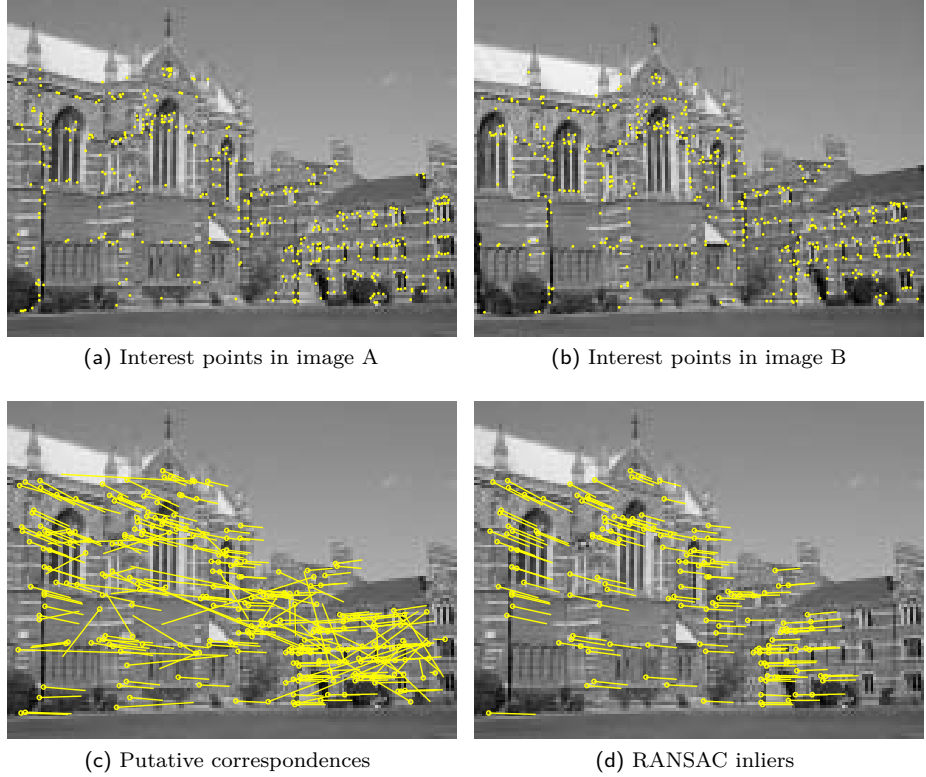


Fig. 3: Robust homography estimation.

- the measurements are independent.

Hence the joint probability density of the set of observed, noisy correspondences $\mathcal{Q} = \{\mathbf{q}_k \leftrightarrow \mathbf{q}'_k\}$, given the set of true, noise-free correspondences $\bar{\mathcal{Q}} = \{\bar{\mathbf{q}}_k \leftrightarrow \bar{\mathbf{q}}'_k = \mathbf{H}\bar{\mathbf{q}}_k\}$, can be expressed as the product of their individual point PDFs

$$\begin{aligned} \mathbb{P}[\mathcal{Q}|\bar{\mathcal{Q}}] &= \mathbb{P}[\{\mathbf{q}_k, \mathbf{q}'_k\}|\mathbf{H}, \{\bar{\mathbf{q}}_k\}] = \prod_k p(\mathbf{q}_k|\bar{\mathbf{q}}_k) p(\mathbf{q}'_k|\bar{\mathbf{q}}'_k) \\ &= \prod_k \frac{1}{2\pi\sigma^2} e^{-d(\mathbf{q}_k, \bar{\mathbf{q}}_k)^2/\sigma^2} \frac{1}{2\pi\sigma^2} e^{-d(\mathbf{q}'_k, \bar{\mathbf{q}}'_k)^2/\sigma^2} \\ &= \prod_k \left(\frac{1}{2\pi\sigma^2} \right)^2 e^{-\left(d(\mathbf{q}_k, \bar{\mathbf{q}}_k)^2 + d(\mathbf{q}'_k, \bar{\mathbf{q}}'_k)^2\right)/\sigma^2} \end{aligned}$$

since the errors on each point are assumed independent.

The negative log-likelihood of the set of all correspondences $L = \ln \mathbb{P}[\mathcal{Q}|\bar{\mathcal{Q}}]$ is therefore²

$$L \propto \sum_k d(\mathbf{q}_k, \bar{\mathbf{q}}_k)^2 + d(\mathbf{q}'_k, \bar{\mathbf{q}}'_k)^2 = \sum_k (x_k - \bar{x}_k)^2 + (y_k - \bar{y}_k)^2 + (x'_k - \bar{x}'_k)^2 + (y'_k - \bar{y}'_k)^2$$

² The unknown scale factor σ be safely dropped in the above equation since it has no effect on the following derivations.

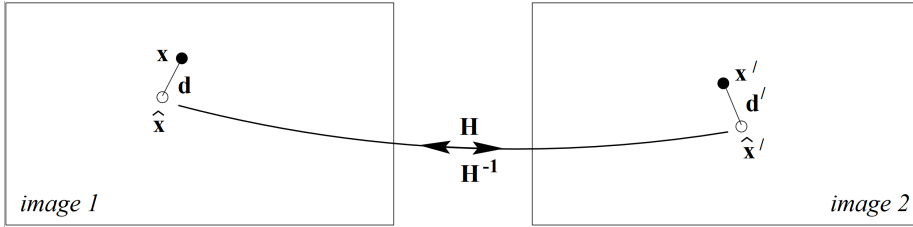


Fig. 4: The points \mathbf{q} and \mathbf{q}' are the measured (noisy) points; under the estimated homography the points \mathbf{q}' and $H\mathbf{q}$ do not correspond perfectly (and neither do the points \mathbf{q} and $H^{-1}\mathbf{q}'$). However, the estimated points, $\hat{\mathbf{q}}$ and $\hat{\mathbf{q}}'$, do correspond perfectly by the homography $\hat{\mathbf{q}}' = H\hat{\mathbf{q}}$.

The additional complication here is that we have to seek “corrected” image measurements that play the role of the true measurements $H\bar{\mathbf{q}}$ above. Thus the ML estimate of the projective transformation H and the correspondences $\{\mathbf{q}_k \leftrightarrow \mathbf{q}'_k\}$, is the homography \hat{H} and corrected correspondences $\{\hat{\mathbf{q}}_k \leftrightarrow \hat{\mathbf{q}}'_k\}$ that minimize [3, p. 103]

$$\sum_k d(\mathbf{q}_k, \hat{\mathbf{q}}_k)^2 + d(\mathbf{q}'_k, \hat{\mathbf{q}}'_k)^2 \text{ subject to } \hat{\mathbf{q}}'_k = \hat{H}\hat{\mathbf{q}}_k \quad (2)$$

Fig. 4 shows the error contribution of a single correspondence $\mathbf{q} \leftrightarrow \mathbf{q}'$. The cost function of Eq. (2) is called *reprojection error*, since we wish to estimate a point \hat{Q}_k in a world planar scene from $\mathbf{q}_k \leftrightarrow \mathbf{q}'_k$ which is then *reprojected* to the estimated perfectly matched correspondence $\hat{\mathbf{q}}_k \leftrightarrow \hat{\mathbf{q}}'_k$ [3, p. 95].³

Since $\hat{\mathbf{q}}' = H\hat{\mathbf{q}}$, minimizing Eq. (2) requires estimating the homography and the set of points $\{\hat{\mathbf{q}}_k\}$: we have to perform a non-linear least square optimization problem over both the 8 parameters of the homography and the $2K$ parameters (\hat{x}_k and \hat{y}_k) of the point set $\{\hat{\mathbf{q}}_k : k = 1 \dots K\}$; for example, the Levenberg-Marquardt algorithm can be used [3, pp. 600-609].⁴

The method provided here for a pair of images is then extended to perform the simultaneous registration of multiple images, in order to obtain globally consistent alignments; however it does not add anything else to the ML criterion, so it is not detailed here (see appendix B for some insights).

3 Super-resolution

The observed low resolution images are regarded as degraded observations of a real, high-resolution image. These degradations typically include geometric warping, optical blur, spatial sampling and noise (see Fig. 5). Given several such low resolution image observations our objective is to solve the inverse problem, i.e. determine the super-resolution image from the measured low resolution images given the image formation model.

³ In the case of a panning/zooming camera, \hat{Q} could be regarded as the intersection with the plane at infinity of the optical rays passing through the camera centre and $\hat{\mathbf{q}}$.

⁴ The Levenberg-Marquardt algorithm is an iteration method moving seamlessly between Gauss-Newton iteration, which will cause rapid convergence in the neighbourhood of the solution, and a gradient descent approach, which will guarantee a decrease in the cost function when the going is difficult.

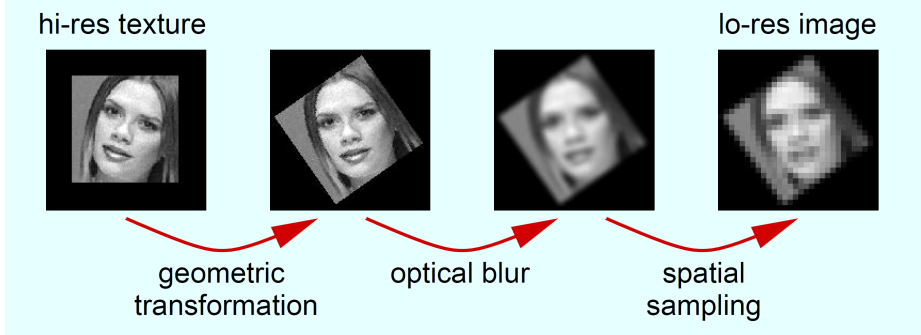


Fig. 5: The principal steps in the imaging model. From left to right: the high-resolution planar surface undergoes a geometric viewing transformation followed by optical/motion blurring and finally down-sampling. In (b):

We will discuss two solutions to this problem:

- in the first, we determine the Maximum Likelihood (ML) estimate of the super-resolution image;
- in the second, we determine the Maximum a posteriori (MAP) estimate of the super-resolution image including prior information.

3.1 Generative model

It is assumed that the set of observed low-resolution images were produced by a single high-resolution image under the following generative model of image formation:⁵

$$g(x, y) = d \downarrow (k(\cdot) * f(T(x, y))) + \epsilon(x, y)$$

being

- f the (ground truth) high resolution image,
- g the observed low resolution image,
- T the geometric transformation mapping the pixel coordinates of g onto f ,
- $k(\cdot)$ the point spread function (PSF), which is a predefined hyper-parameter of the model (blur modeled as pixel local average, see Fig. 6),
- $d \downarrow$ the down-sampling operator
- ϵ noise in each image.

Such a model can be expressed in matrix form as

$$\mathbf{g} = \bar{\mathbf{M}}\mathbf{f} + \boldsymbol{\epsilon}_n \quad (3)$$

in which the vector \mathbf{f} is a lexicographic reordering of pixels in $f(x, y)$ and the operators $d \downarrow$, T and $k(\cdot)$ have been combined into a single matrix $\bar{\mathbf{M}}$ following the scheme of Fig. 7 [1, pp. 122-129], i.e.:

$$\mathbf{M} = \bar{\mathbf{M}}\mathbf{T}^{-1}$$

⁵ With respect to [1, 2], the photometric component of the model is omitted for brevity.

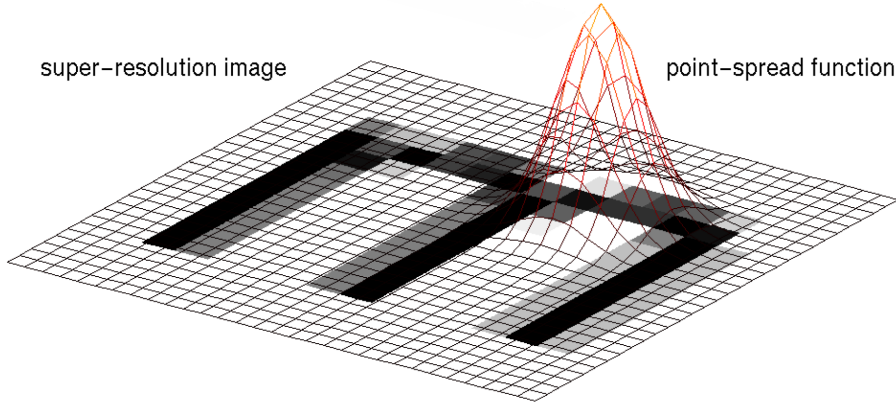


Fig. 6: Point spread function (PSF) using a Gaussian kernel.

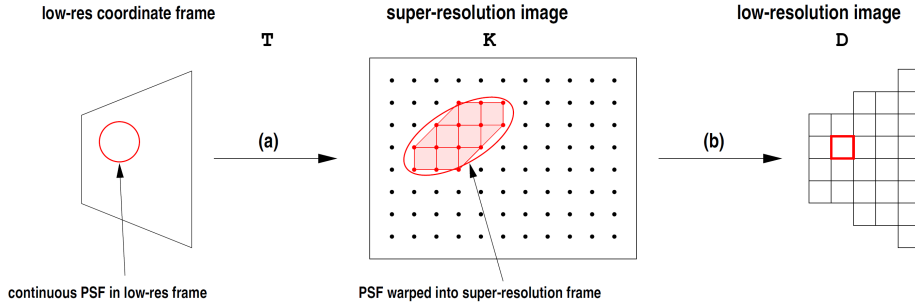


Fig. 7: The principal steps to compute matrix M in Eq.3.

being

- D the discrete down-sampling (decimation) matrix,
- K the convolution matrix formed from discretization of the warped $k(\cdot)$,
- T the geometric warp from g to f .

Looking at Eq.3, each low-resolution pixel is therefore a linear combination of super-resolution pixels, where the super-resolution pixels acts as weights of the *observed elements* in matrix M_n determined by the registration parameters, and the shape of the point-spread function, and spatial sampling.

3.2 Probabilistic framework

3.2.1 Maximum Likelihood solution

According to Eq.3, let $\hat{g} = M\hat{f}$ the low resolution image produced by an estimate \hat{f} of the super-resolution image, and assume the image noise in each point of the observed g to be Gaussian with mean zero, variance σ_ϵ^2 (i.e $\epsilon \sim N(0, \sigma_\epsilon^2)$). Thus we can write for a single pixel value of g in (x, y)

$$p(g(x, y) | M, \hat{f}, \epsilon) = \mathcal{N}(g(x, y) | M\hat{f}, \epsilon) = \frac{1}{\sqrt{2\pi\sigma_\epsilon^2}} \exp\left(\frac{(g(x, y) - \hat{g}(x, y))^2}{2\sigma_\epsilon^2}\right) \quad (4)$$

Under the (simplified) assumption of i.i.d. samples, the likelihood of the overall image g , given \mathbf{M} and \hat{f} can be written as

$$L_g = \mathbb{P}[g|\mathbf{M}, \hat{f}, \epsilon] = \prod_{(x,y) \in g} p(g(x,y)|\mathbf{M}, \hat{f}, \epsilon)$$

Hence, taking the logarithm

$$\begin{aligned} \ln L_g &= \sum_{(x,y) \in g} \ln p(g(x,y)|\mathbf{M}, \hat{f}, \epsilon) \\ &= \alpha - \frac{1}{2\sigma_\epsilon^2} \sum_{(x,y) \in g} (g(x,y) - \hat{g}(x,y))^2 \\ &= \alpha - \frac{1}{2\sigma_\epsilon^2} \|\mathbf{g} - \mathbf{M}\hat{\mathbf{f}}\|^2 \end{aligned} \quad (5)$$

where α can be regarded as a constant since not depending from \hat{f} . This means that maximizing L_g is equivalent to minimize $\|\mathbf{g} - \mathbf{M}\hat{\mathbf{f}}\|^2$.

Assuming again independent observations, the likelihood over all the whole set of N images $\{g_n\}$ is given by $L = \prod_n L_{g_n}$ and is maximized for⁶

$$f_{\text{MLE}} = \arg \min_f \sum_n \|\mathbf{g}_n - \mathbf{M}_n \mathbf{f}\|^2 \quad (6)$$

where \mathbf{M}_n is the matrix model for image g_n .

Eq. (6) is equivalent to solve the generative model of all N images obtained by stacking vertically the single-image generative model to form a “standard” over-determined linear system

$$\underbrace{\begin{bmatrix} \mathbf{g}_1 \\ \mathbf{g}_2 \\ \vdots \\ \mathbf{g}_N \end{bmatrix}}_{\mathbf{g}} = \underbrace{\begin{bmatrix} \mathbf{M}_1 \\ \mathbf{M}_2 \\ \vdots \\ \mathbf{M}_N \end{bmatrix}}_{\bar{\mathbf{M}}} \mathbf{f} \quad (7)$$

whose solution is

$$f_{\text{MLE}} = (\bar{\mathbf{M}}^\top \bar{\mathbf{M}})^{-1} \bar{\mathbf{M}}^\top \mathbf{g}$$

Note anyway that $\bar{\mathbf{M}}$ in Eq. 7 is a (huge) sparse matrix, since each \mathbf{M}_n is already sparse, so the solution can not be computed by standard matrix factorizations: instead, iterative methods such as preconditioned conjugate gradient descent can be applied.

Some examples of MLE results are shown in Figs. 8-9. As the zoom factor increases further characteristic high frequency noise is superimposed on the super-resolution image. This is a standard occurrence in inverse problems and results from noise amplification due to poor conditioning of the $\bar{\mathbf{M}}$. One standard remedy is to regularize the solution, and this is discussed in the next section where the regularizers are considered as prior knowledge

⁶ Since $\arg \max L = \arg \max \ln L = \arg \max \sum \ln L_{g_n}$.

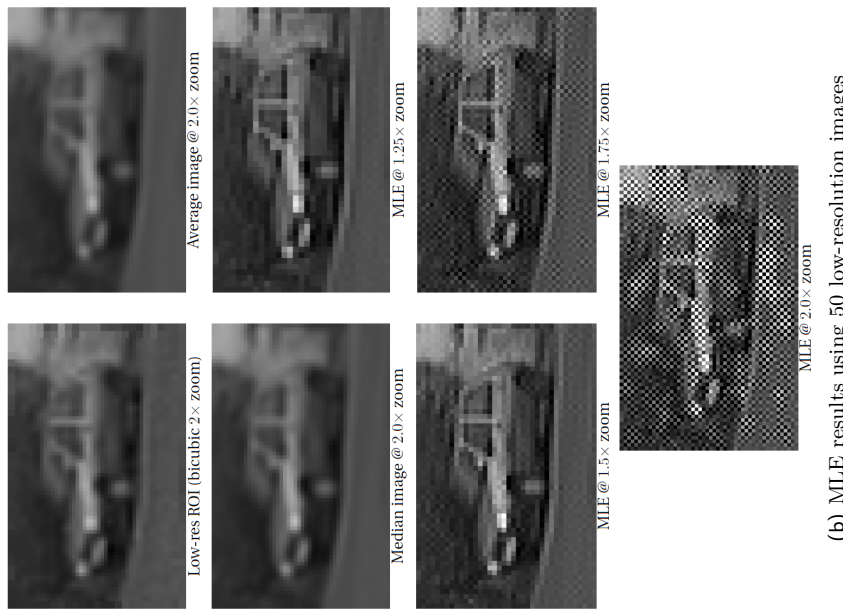


Fig. 8: Car Example
.



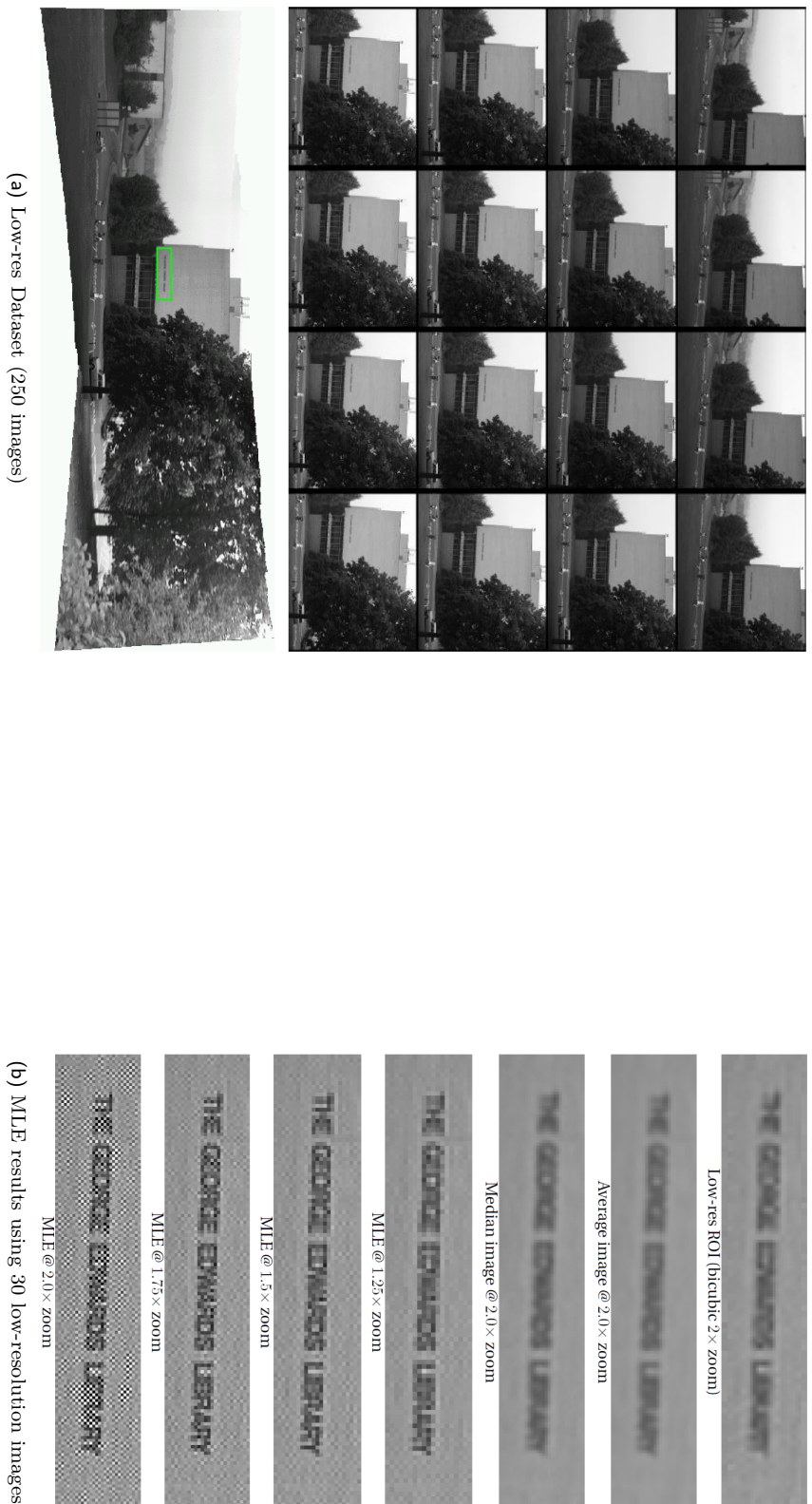


Fig. 9: Library Example

3.2.2 Maximum a posteriori solution

Suppose we have prior information $\mathbb{P}[\hat{\mathbf{f}}]$ on the form of the super-resolution image. By applying Bayes theorem, the posterior probability $\mathbb{P}[\hat{\mathbf{f}}|\mathbf{g}]$ is

$$\mathbb{P}[\hat{\mathbf{f}}|\mathbf{g}] = \frac{\mathbb{P}[\mathbf{g}|\hat{\mathbf{f}}] \mathbb{P}[\hat{\mathbf{f}}]}{\mathbb{P}[\mathbf{g}]}$$

where the likelihood $\mathbb{P}[\mathbf{g}|\hat{\mathbf{f}}]$ is given in Eq. (5). The maximum a-posterior (MAP) estimate of \mathbf{f} is then obtained as

$$\begin{aligned} \mathbf{f}_{\text{MAP}} &= \arg \max_{\mathbf{f}} \ln \mathbb{P}[\mathbf{f}] + \ln \mathbb{P}[\mathbf{g}|\mathbf{f}] \\ &= \arg \max_{\mathbf{f}} \ln \mathbb{P}[\mathbf{f}] - \frac{1}{2\sigma_e^2} \|\mathbf{g} - \mathbf{M}\hat{\mathbf{f}}\|^2 \end{aligned}$$

The specific form of $\ln \mathbb{P}[\mathbf{f}]$ depends on the prior being used, and we will now overview a few popular cases in the family

$$\mathbb{P}[\mathbf{f}] = \frac{1}{Z} \exp(-\mathbf{f}^\top \mathbf{Q} \mathbf{f}) \quad (8)$$

where \mathbf{Q} is a symmetric, positive-definite matrix. In this case, the MAP estimator

$$\mathbf{f}_{\text{MAP}} = \arg \max_{\mathbf{f}} -\mathbf{f}^\top \mathbf{Q} \mathbf{f} - \frac{1}{2\sigma_e^2} \|\mathbf{g} - \mathbf{M}\hat{\mathbf{f}}\|^2$$

has, in principle, a linear solution:

$$\mathbf{f}_{\text{MAP}} = (\mathbf{M}^\top \mathbf{M} + \mathbf{Q})^{-1} \mathbf{M}^\top \mathbf{g}$$

Of course, in the context of image restoration, it is computationally infeasible to perform the matrix inversion directly, and the solution must be computed by iterative methods (e.g. conjugate gradient ascent method).

3.2.3 Markov Random Field priors

The image priors considered in this work are simple Markov Random Field (MRF) models⁷, based on heuristic notions about the short-range spatial correlations between pixels in typical images [1, p. 178]: in other words, the conditional pdf of a single pixel, conditioned on all other pixels in the image, is equal to the pdf conditioned on just some sub-set of the other pixels [1, p. 180].

In MRF image models, the pixel neighbourhoods are typically determined by some spatial adjacency rule. The prior in Eq. 8 is the simplest and most common form of distribution for a MRF.

Gaussian Prior Assuming zero-mean Gaussian i.i.d. pixel values, the associated prior is

$$\mathbb{P}[\mathbf{f}] = \frac{1}{Z} \exp\left(-\frac{\|\mathbf{f}\|^2}{2\sigma_f^2}\right)$$

⁷ The majority of priors in the image restoration literature, are Markov Random Fields [1, p. 180].

Since

$$\ln \mathbb{P}[\mathbf{f}] = -Z - \frac{\|\mathbf{f}\|^2}{2\sigma_f^2} = -Z - \frac{\mathbf{f}^\top \mathbf{f}}{2\sigma_f^2} = -Z - \frac{\mathbf{f}^\top \mathbf{I} \mathbf{f}}{2\sigma_f^2}$$

in this case we have $\mathbf{Q} \propto \mathbf{I}$, i.e. an example of Tikhonov regularization:

$$\mathbf{f}_{\text{MAP}} = \arg \max_{\mathbf{f}} -\gamma \|\mathbf{f}\|^2 - \frac{1}{2\sigma_\epsilon^2} \|\mathbf{g} - \mathbf{M}\hat{\mathbf{f}}\|^2$$

In general if \mathbf{Q} in Eq. (8) is the covariance matrix of a multivariate Gaussian distribution over \mathbf{f} in which spatial correlations between adjacent pixels are captured by the off-diagonal elements, the corresponding MRFs are termed Gaussian MRFs or GMRFs: another special case is obtained for $\mathbf{Q} = \mathbf{L}^\top \mathbf{L}$ with \mathbf{L} formed by taking first-order finite difference approximations to the image gradient over horizontal, vertical and diagonal pair-cliques, yielding another example of Tikhonov regularization, i.e.

$$\mathbf{f}_{\text{MAP}} = \arg \max_{\mathbf{f}} -\gamma \|\mathbf{L}\mathbf{f}\|^2 - \frac{1}{2\sigma_\epsilon^2} \|\mathbf{g} - \mathbf{M}\hat{\mathbf{f}}\|^2$$

Huber MRFs A common criticism levelled at the GMRF priors is that the associated MAP super-resolution estimates tend to be overly smooth, and that sharp edges, which are what we are most interested in recovering, are not preserved. This problem can be ameliorated by modelling the image gradients with a distribution which is heavier in the tails than a Gaussian. Such a distribution accepts the fact that there is a small, but nonetheless tangible probability of intensity discontinuities occurring.

In a Huber MRF (HMRF) the prior of \mathbf{f} is Gaussian close to the origin, becoming Laplacian in the tails (Fig. 10):

$$p(x) = \frac{1}{Z} \exp(-\gamma\rho(x))$$

where x is the 1st derivate of the image, and $\rho(x)$ is the Huber function

$$\rho(x) = \begin{cases} x^2 & (|x| < \alpha) \\ 2\alpha|x| - \alpha^2 & (\text{else}) \end{cases}$$

Fig. 11a compares the results obtained under these three priors for the car example. The MAP solutions at $3\times$ pixel zoom show more convincing detail than the ML reconstruction of Fig. 8, especially around the door handles and wing mirror. The Gaussian priors produce similar results, but note the sharp edges around the windows and headlights in the HRMF reconstruction. Furthermore, the priors have eliminated the noise of the ML solution, without introducing artifacts of their own. A ML solution at this zoom-factor would be completely dominated by noise.

Again in Fig. 11b, the superiority of the MAP results over the MLE is quite convincing. The HMRF estimator is particularly effective at reconstructing the sharp edges of the letters in this example. The text is clearly legible, which is certainly not the case in the low-resolution input.

Finally, Figs. 12-fig:Mars show another two examples of hi-res reconstructed images.

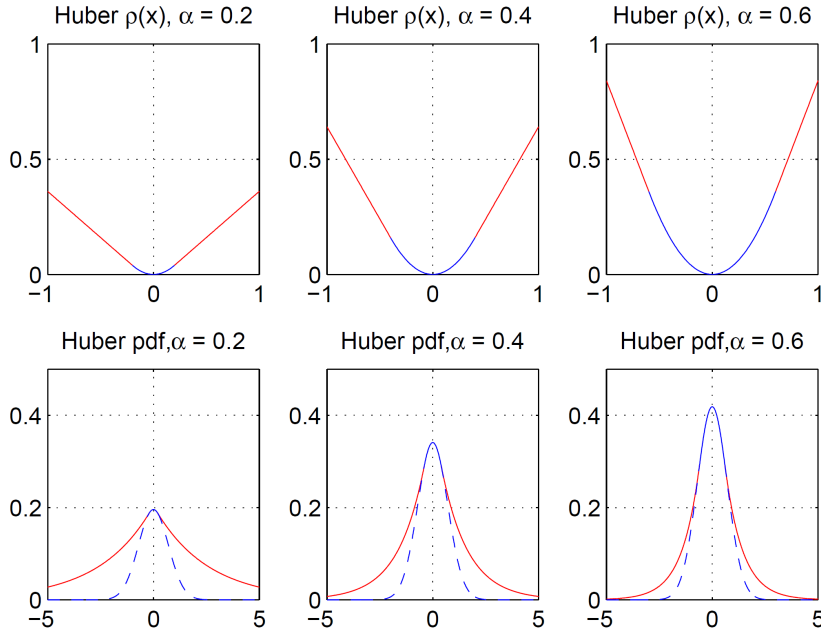


Fig. 10: (Top) The Huber potential functions $\rho(x)$, plotted for three different values of α . (Bottom) The corresponding distributions are a combination of a Gaussian (dashedline) and a Laplacian distribution.

A Homogeneous representation of homographies

By representing Cartesian points in homogeneous coordinates, so that a point (x, y) is represented as $(x, y, 1)$ (and conversely the point (q_1, q_2, q_3) in homogeneous coordinates corresponds to the inhomogeneous point $(q_1/q_3, q_2/q_3)$), Eq. (1) can be formulated in matrix form as

$$\underbrace{\begin{bmatrix} q'_1 \\ q'_2 \\ q'_3 \end{bmatrix}}_{\mathbf{q}'} = \underbrace{\begin{bmatrix} h_{11} & h_{12} & h_{13} \\ h_{21} & h_{22} & h_{23} \\ h_{31} & h_{32} & h_{33} \end{bmatrix}}_{\mathbf{H}} \underbrace{\begin{bmatrix} q_1 \\ q_2 \\ q_3 \end{bmatrix}}_{\mathbf{q}}$$

where equality is defined up to a scalar factor.

B Simultaneous registration of multiple images

The two-view maximum likelihood estimator may be easily extended to perform simultaneous registration of any number of views:

- let, in image n , \mathbf{q}_k^n the k -th observed noisy point from a world point \bar{Q}_k (note that \bar{Q}_k may be observed in several (but not necessarily all N) images);
- the estimated “real” points \hat{Q}_k are explicitly parameterized to lie in an arbitrarily chosen *reference plane*;

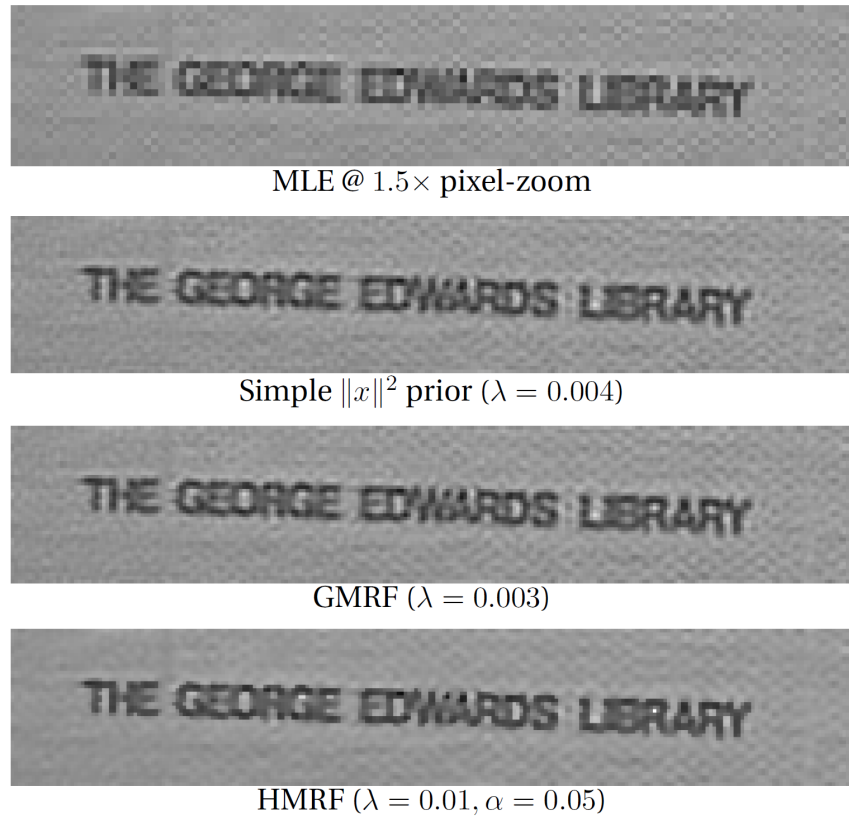
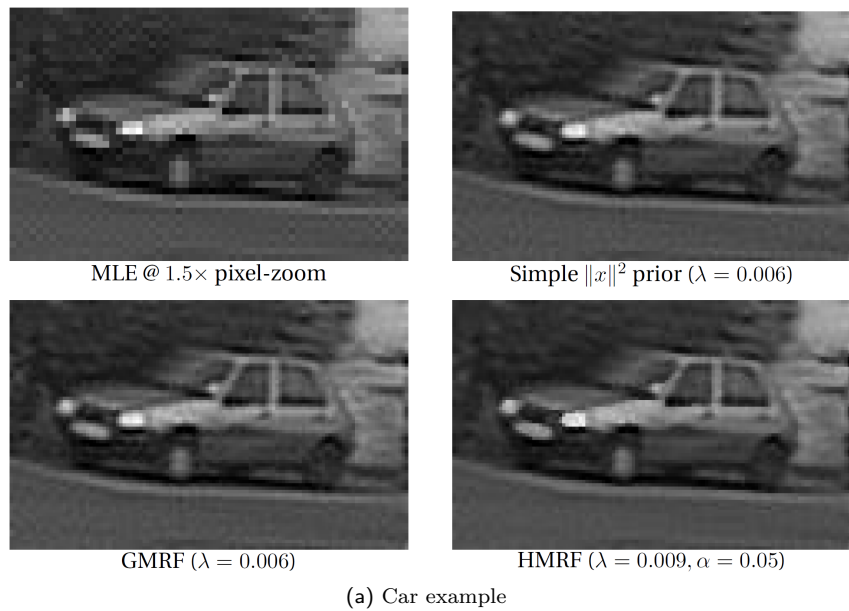


Fig. 11: MAP Examples.

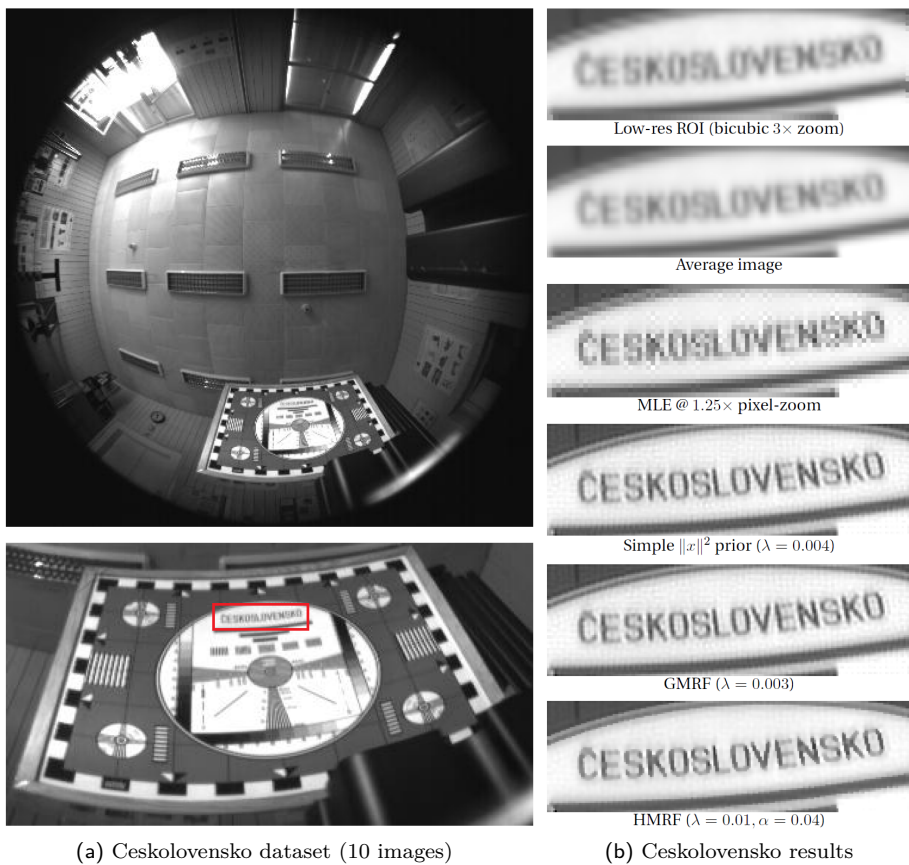
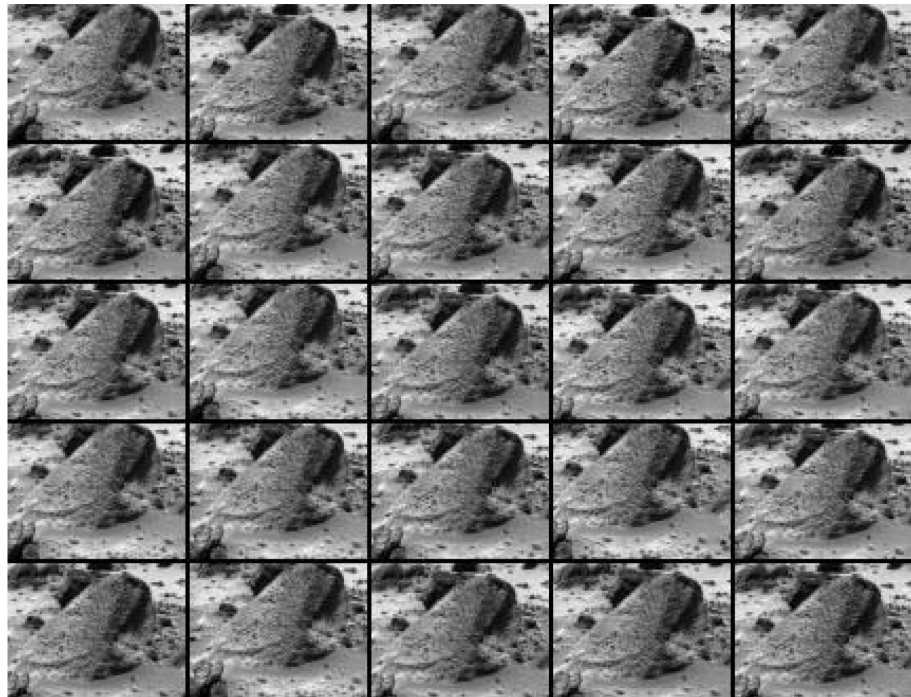


Fig. 12: Hi-res images for Ceskolovensko sequence.



(a) Mars dataset (25 images)



MLE @ 1.5x zoom

(b) Mars MLE

GMRF ($\lambda = 0.01$)

(c) Mars MAP (3x zoom)

Fig. 13: Hi-res images for Mars sequence.

- for each image n the homography \mathbf{H}_n projects $\hat{\mathbf{Q}}_k$ onto its image point $\hat{\mathbf{q}}_k^n = \mathbf{H}_n \hat{\mathbf{Q}}_k$;
- analogously to the two-view ML estimator, the N -view estimator minimizes the (squared) geometric distances $d(\mathbf{q}_k^n, \hat{\mathbf{q}}_k^n)$ between each observed feature point \mathbf{q}_k^n and its predicted position $\hat{\mathbf{q}}_k^n = \mathbf{H}_n \hat{\mathbf{Q}}_k$;
- in practice one of the images is selected to be the reference plane.

This guarantees that the estimated homographies will be globally consistent.

Riferimenti bibliografici

- [1] David P. Capel. *Image Mosaicing and Super-resolution*. PhD thesis, University of Oxford, 2001.
- [2] David P. Capel and Andrew Zisserman. Computer vision applied to super resolution. *IEEE Signal Processing Magazine*, 20(3):75–86, 2003.
- [3] Richard I. Hartley and Andrew Zisserman. *Multiple View Geometry in Computer Vision*. Cambridge University Press, second edition, 2004.